Recyclability of stainless steel (316 L) powder within the additive manufacturing process

Nima E. Gorji [a,*], Rob O'Connor [a], Andre Mussatto [a], Matthew Snelgrove [a], P.G. Mani González [a,b], Dermot Brabazon [a]

[a] *I-Form Additive Manufacturing Research Centre, Dublin City University, Dublin 9, Ireland*
[b] *Institute of Engineering and Technology, Department of Physics and Mathematics, Autonomous University of Ciudad Juarez, Cd. Juarez, Mexico*

Abstract

Using recycled powder during the additive manufacturing processes has been a matter of debate by several research groups and industry worldwide. If not significantly different from the feedstock, the recycled powder can be reused many times without a detrimental impact on the mechanical properties of the final printed parts, which reduces the metallic powder waste and printing time. A detailed characterization and comparison of the feedstock and recycled powders is essential in order to understand the number of times a powder can be recycled. The recycled powders were sampled after 10 times reuse in the Powder Bed Fusion (PBF) process in the 3D printer. In this paper, we have performed a detailed characterization on morphology, microstructure, and the surface and bulk composition of virgin feedstock and recycled stainless steel 316 L powders (over 10 times reused), and correlated these measurements to topography, nanoindentation and hardness tests. We have also performed rarely reported synchrotron surface characterization of both powder sets in order to measure the level of oxidation of the individual metallic elements present in the virgin and recycled steel powder and the way such chemical composition changes following use in the manufacturing process. The results show more satellite and bonded particles in the recycled powder although the particle size is not broadly impacted. The atomic force microscopy results showed a smaller roughness on recycled powders measured on surfaces without satellites which might be due to less surface dendrites on recycled powder surface. Finally, a higher hardness was measured for the recycled powder resulted from the manufacturing process on grains and chemical composition. The results suggest no significant changes on the mechanical properties of the printed parts depending for a certain number of reusing cycles.

* Corresponding author.
E-mail addresses: nima.gorji@i-form.ie, Nima.gorji@dcu.ie (N.E. Gorji), Rob.oconnor@dcu.ie (R. O'Connor), andre.mussatto2@mail.dcu.ie (A. Mussatto), matthew.snelgrove2@mail.dcu.ie (M. Snelgrove), pierre.mani@uacj.mx (P.G.M. González), Dermot.brabazon@dcu.ie (D. Brabazon).

1. Introduction

Recently, Additive Manufacturing (AM) of metallic parts for a wide range of applications ranging from dental implants to aviation industry has been the focus of many research groups and industry [1]. In order to reduce the materials consumption/waste, the consumed energy and the production cost, the reusability of the recycled powder in each printing cycle requires detailed examination. This provides an understanding of the impact of reusing the recycled powder on the final part characteristics. For some industries, e.g. for risk intolerant aviation industry, it is inevitable to ensure the component's high quality especially of the parts printed from recycled powders [2]. However, not many research has been presented in literature on characterization of surface, bulk, and microstructure of the recycled metallic powders printed by commercial 3D printing machines for different applications [3]. Inconnel, Ni-Ti, Co-Cr, and stainless steel are the core of such research in literature. Nandwana et al. have reported that the reuse of Inconel 718 and Ti-6Al-4 V is governed by the oxygen pick up of the powder during/between build cycles [4]. Tang et al. presented that the recycled Ti-6Al-4 V can be reused for 21 times with insignificant effect on the mechanical properties of the AM printed tensile bars. However, they reported the Oxygen increment on reused powder progressively by reuse times [5]. Similarly, Simonelli et al. have also noticed an increased surface oxidation on stainless steel 316 L (SS316L) and Al-Si10-Mg by repeated use in the Bed Fusion (PBF) process [6]. Electron-dispersive spectroscopy (EDS) by Jelis et al. on Steel 4340 revealed an increased Oxygen level on powder surface and assigned that to changes in Oxygen level in the PBF chamber [7]. Similar to above studies, National Institute of standards and technology (NIST) has also confirmed that reusing the recycled Stainless Steel S17-4 pH powders for 11 times will not change the tensile strength of the parts

dramatically [8]. Hann (from Honeywell Aerospace) has also reported that reusing the Ni-based super-alloy 718 powder for 10 times showed no appreciable impact on mechanical properties but the Oxygen content was gradually increased [9].

In this paper, our focus is on recyclability of stainless steel 316 L (SST316L) powder during the AM process. Sartin et al. have reused the SS316L powder for 12 times and concluded that only 5% of the powders are subject to variations in oxidation level, size and microstructure [10]. Conversely, Terrassa et al. reported that change on powder surface/bulk properties (e.g. Oxygen level increment) comes from laser interaction and printing condition together [11]. They, however, reported insignificant changes occur on mechanical properties of the printed parts after 9 reuse. Heiden et al. reported the Oxidation level increases by build

cycles and thus the printed part's density decreases slightly for higher reusing times but the yield strength remains relatively consistent [12]. Independently, Galicki et al. reported that the oxygen picks up of the unmelted powder varies as function of its relative position to the heat source and the spatter ejecta in molten materials have highest oxidation rate [13]. Barnhart et al. have reported higher oxygen concentration on the surface of reused powder compared to virgin after 4 reuse times but a slight change on tensile of the printed parts [14].

Here, we report our latest characterization on surface composition, morphology, topography and microstructure tests on both virgin and recycled SST316L powders and correlate the characterization results to hardness of the powder in order to asses if the recycled powder can be still reused in the 3D printing process. These studies also shed light on
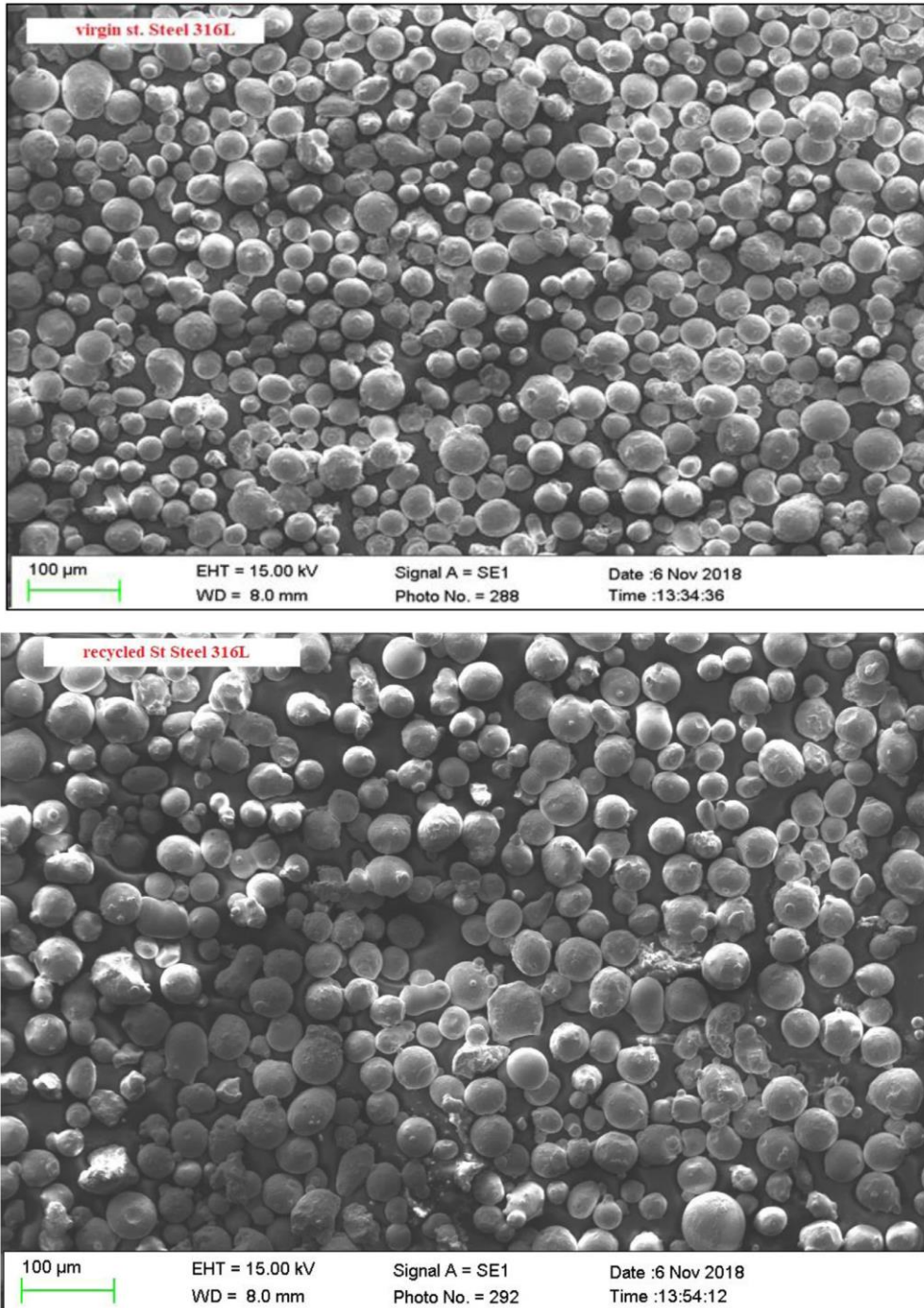

Fig. 1. SEM images of both virgin (left) and recycled (right) SST316L powders at 100 μm. The virgin powder shows more spherical and less fine particles than the recycled powder with deformed contaminated shape and many finer particles.

the need to mix the recycled powder with fresh feedstock during the manufacturing process.

2. Materials and characterization methods

The commercial gas-atomized powders stainless steel alloy 316 L powder used in these experiments was manufactured and delivered from a commercial supplier [Castolin Eutectic - Ireland]. The average particle size used was 75μm. However, finer or bigger particles do also exist. However, the particle size distribution is not broad as confirmed with our rheology Malvern Mastersize analyzer. About 1 kg of the recycled powders was sieved for particles bigger than 75 μm before characterization, however, some spatters were still present in sieved. The exact number of times these powders were recycled has not been recorded but it is definitely over 10 times. The AM parts 5 cm^3 cubes were produced using the virgin powder in the EOSINT M280 SLM 3D printer (powder bed fusion process) with 195 W power, 1000–1200 mm/s scan velocity, 0.1% limit on O_2 in AM chamber, 80 °C ambient temperature and 0.1 mm beam diameter. The powder was collected by vacuum cleaner taken over the whole powder bed. We performed several detailed characterizations on the surface structure, bulk, size, microstructure of both virgin and recycled powders to understand how the chemical composition and mechanical properties of the powders change during the AM process. The hardness and roughness were also measured on both powders using the Nanoindentation and Atomic force microscopy measurements, respectively.

2.1. Size and shape morphology analysis

We performed scanning electron microscopy (SEM) using EVO-LS15 Scanning Electron Microscope and also high-resolution SEM measurements using (Hitachi S5500 Field Emission SEM) to survey the change in size, grains, surface contamination, morphology and microstructure of the powder particles.

2.2. Surface composition analysis

We performed X-ray Photoemission Spectroscopy (XPS) to analyze the surface composition of the powders using a VG Microtech electron spectrometer, at base pressure of 10^{-9} mbar, and a conventional Mg Kα (hν = 1253.6 eV) X-ray source. The XPS curves were fitted using CASAxps software. The binding energy positions were referenced to the C 1 s peak at 284.5 eV. No chemical treatments were conducted on the particles prior to XPS scans in order to reduce the surface contamination. We manually sprinkled powders on an adhesive carbon pad mounted on a 1 cm^2 diameter steel circular sample holder. The acquired XPS peaks were curve-fitted to their relevant chemical species using literature values and the NIST X-ray Photoelectron Spectroscopy Database.

2.3. HAXPES synchrotron analysis

Hard X-Ray Photoelectron Spectroscopy (HAXPES) measurements at the SOLEIL Synchrotron were carried out on the Galaxies Beamline [15]. Spectra were acquired at pressures of 1×10^{-9} mbar with photon beam energy of 10k eV, which allows for probing of deep core levels of all elements present as well as the acquisition of more bulk sensitive (10k eV) spectra. A Si (333) monochromator was used for 10k eV beam. Both virgin and recycled powders were measured under these conditions.

2.4. Atomic force microscopy (AFM) roughness

To measure the roughness of the virgin and recycled powder particles, we performed Atomic Force Microscopy (AFM) and confocal microscopy using the Bruker Dimension ICON AFM. The scan tube size is 90 μm, which is coupled with a TESPA cantilever of 8 nm tip radius. Tapping mode was applied and powder particles were sprinkled on moulds. The analysis area was 10 μm^2 and several particles mounted on moulds were analyzed. The AFM topological images were taken on the polished area of the particle. The images were plane leveled with the noise reduction filter (medium) enabled in Gwyddion software. The Median Filter is a non-linear digital filtering technique, often used to remove noise from an image or signal.

2.5. Nanoindentation and hardness test

Finally, we performed Nanoindentation hardness tests on both powders using Bruker HYSITRON TI Premier. For this experiment, we used cold mounting of the powder particles using two round moulds silicon rubbers. The mounted particles were then polished in micro and nano
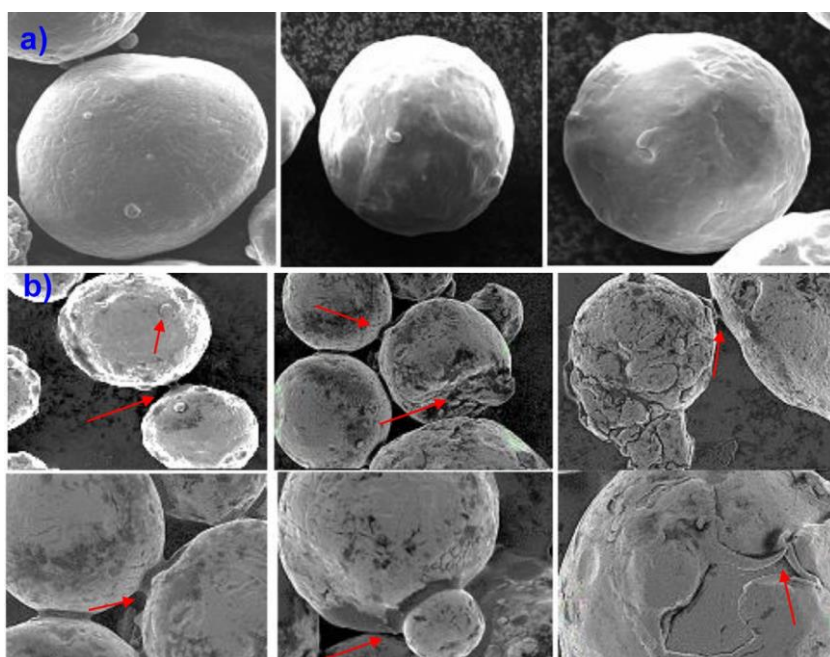

Fig. 2. High-resolution SEM images of the (a) virgin particles and (b) recycled powder particles showing the bonding of the particles, surface cracks and contamination, satellites, clustering of the particles and the surface quality. (**all images in 10 μm scale**).

Table 1
Concentration of chemical elements on powder surface extracted from XPS curves using CasaXPS.

Powder	%O	%C	%Mn	%Fe	%Si	%Sb	%Cu
Virgin	27.04	56.21	2.02	1.04	10.83	2.86	–
Recycled	34.19	45.55	2.27	2.70	10.07	–	5.22

size using the diamond suspensions. MetPrep Tri Hard solution and powder was used as the based materials and we polished the particles using Metkon Forcipol polisher and using Diamond Suspension 6 and 1 μm and then using Silicon Colloidal Silica 0.06 μm. The optical microscope was used to scan the polished surface of the particles at every stage.

3. Results and discussions

3.1. Morphology of the powders

The SEM images of the powder particles shows the grain size, shape, surface contamination and porosity of the particles before and after SLM processing. The powders were sieved for bonded and agglomerated particles larger than 75 μm. However, still some particles or spatters exist in sieved powder with irregular shape and bigger size than the mesh or grown like thin bar are found in the powder under SEM (Fig. 1). Our Image processing results (not shown here) by ImageJ free source software shows that the size of the recycled powder has not change dramatically and the particles have mostly retained their spherical shapes. The powder particles average size for virgin and recycled powder was 75 μm and 80 μm, respectively. This is not surprising since many literature have reported that even after many (i.e. 20 or 30) reuse times, the average particle size increases only slightly [4,16]. Nevertheless, the number of fine particles with diameter <10 μm reduces and the number of larger particles increases which broadens the Gaussian distribution of the volume fraction of reused particles. This broader distribution is due to existence of larger particles and either the finer particles which are fewer than compared to larger ones. The recycled powder shows lots of bonded particles, fused particles, and cluster formation with more satellites on particles and some particles with deformed shape. Some particles in the recycled powder now show a smoother surface than the virgin powder. Heiden et al. suggested that the heat affects some particles during the melting and solidification that shatters their rough surface [12]. We also show several virgin particles with much cleaner circular surface for comparison. Some recycled powder particles show noticeable signs of porosity and cracks on the surface as shown in Fig. 2b. Conversely, Heiden et al. reported a reduction in both surface and internal pores in reused powder particles suggesting that pores break up with under the laser's heat and the porous particles are consumed by time [12].

3.2. Surface composition

The XPS results presented for both powder sets indicate significant oxidation of the recycled powder and the presence of metallic oxides on the surface compared to virgin powder (Fig. 3). Table 1 compares the elemental composition of the surface of virgin and recycled powder calculated using CasaXPS software. While the survey spectra in Fig. 3a are dominated by carbon and oxygen, which are typically observed at the surface of stainless steel powder grains, the results also show the presence of Mn, Cu, Fe, Cr, Ni, and Si on both powders. There are significant differences in elemental concentrations between the virgin and recycled powders, which is in agreement with literature [17]. The most notable changes are the increase in oxygen content (27.0% to 34.24%) and reduction in carbon concentration (56.2% to 45.6%). These results are in agreement with the literature reports [18] of the metallic signals observed, Mn (640 ev) and Fe (at 708 eV) peaks are the most prevalent in both powders and are slightly more intense for recycled powder. Heiden et al. have also reported the same peaks but also a weak Cr peak
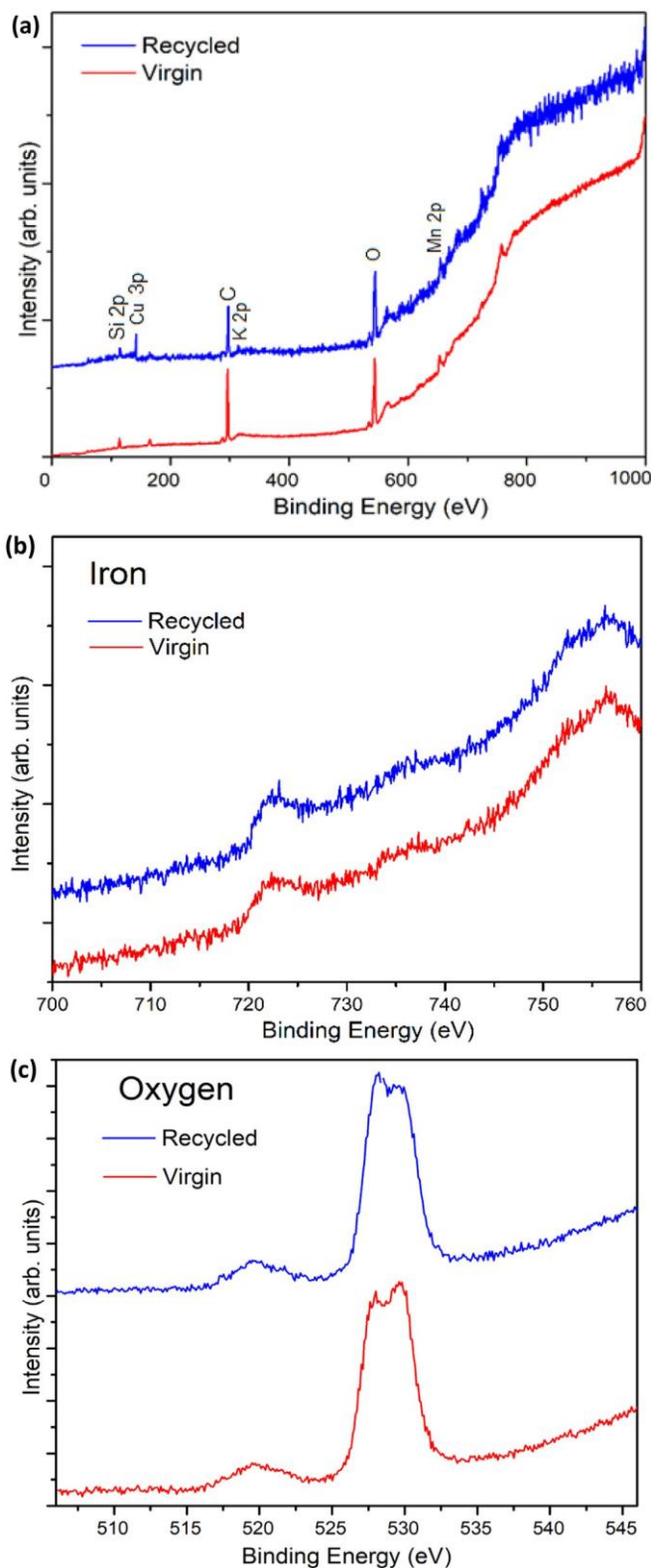

Fig. 3. XPS spectra of the virgin and recycled SST316L powders acquired using lab based XPS. The wide energy range survey scans (a) show that the spectra are dominated by carbon and oxygen, which make up 83% and 80% of the total signal for the virgin and recycled powders, respectively. This is due to the adsorption of oxidized adventitious carbon containing species on the surface (b) shows the Fe 2p spectra. Little information about the chemical state of the iron can be extracted due to the surface contamination. (c) Oxygen Spectra.
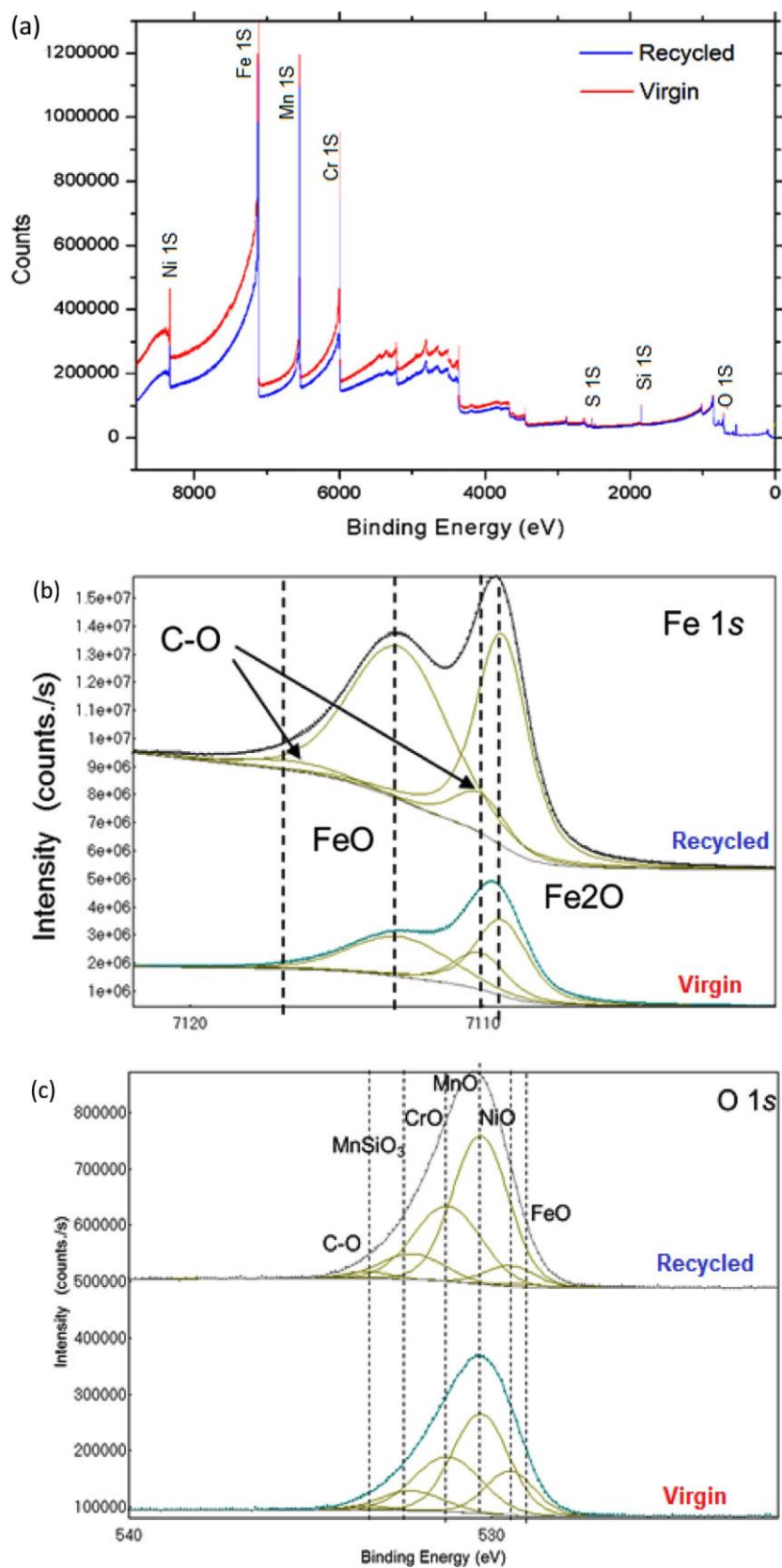
Fig. 4. HAXPES Synchrotron analysis of both virgin and recycled SST316L powders. Survey spectra (a) are dominated by metallic core level peaks. (b) The sharp Fe 1 s signal allows for fitting with the component peaks in order to understand the oxidation state of the Fe. The O 1 s spectra (c) show that the signals associated with Fe, MnSiO₃, and Cr increase for the recycled powder while Ni signal decreases.

(at 574 eV) which is not observed in our XPS measurements [12]. This could be attributed to the degree of contamination observed. Note that even the Fe 2p in Fig. 3b is difficult to differentiate from the background noise.

Based on the increased oxygen concentration and corresponding reduction in carbon, we conclude that the metallic oxides form during the AM process and oxide thickness increases on surface. The shape and intensity of the Fe 2p peaks is similar in both powders (Fig. 3b) showing that the iron oxide species are present on surface regardless of powder recycling, but a detailed analysis of the oxidation state proves difficult. Conventional XPS measurements show some changes in the O 1 s peak (Fig. 3c) in the recycled powder; however, detailed analysis of this peak is difficult due to the limited resolution of the lab-based XPS system. Three iron species, which consisted of pure metal (707 eV) and metal oxide species (710 eV and 712 eV), were identified to fit with several peaks. Several possible metal oxide species are: FeO (709.6 eV), Fe_2O_3 (710.9 eV), and FeS (711.9 eV).

3.3. HAXPES synchrotron measurements

In order to better understand the chemical composition of the near surface region and the effect of the AM process on the oxidation states of the metallic elements near the surface, Hard XPS (HAXPES) measurements were performed at the SOLEIL synchrotron, Paris. The HAXPES synchrotron results are shown in Fig 4. HAXPES measurements correlate with and enhance the non-monochromatic XPS source results, indicating the presence of metallic oxides on the surface. The survey spectra (Fig. 4a) are not dominated by carbon and oxygen, but by sharp signals attributable to the 1 s core levels of metallic elements, showing that the increased sampling depth of HAXPES allows for probing of the steel powder grains beyond the surface region, which is primarily composed of contaminant elements.

The Fe 1 s spectra in Fig. 4b shows two signals present; the Fe^{1+} signal was identified at 7109.3 eV, while the Fe^{2+} signal was recorded at 7112.8 eV. This suggests that at the surface, the Fe^{2+} is the predominant signal for the recycled powder. The Cr 1 s signal obtained suggests that Cr^{1+} at 5987.5 eV is more predominant at the recycled powder surface. The manganese oxide signal decreases while the silicate signal increases, which indicates that the silicon has occupied the manganese on the surface.

The high-resolution O 1s-spectra fits in Fig. 4c show six signals are required in order to accurately fit the data. The component at the lowest binding energy (529.3 eV) is associated with Iron oxide [19]. The peak at 529.46 eV is associated with Nickel oxide, which shows a decrease in the recycled powder [20]. This decrease is also observed for Ni 1 s signal (not shown). The peak at 530.27 eV was associated with Mn oxide. Table 2 shows the relative change in the elements concentration (ΔC) from the signal detected for each element in the recycled powder when compared with the virgin sample. As expected, the oxygen content rises for the recycled sample. Fe, Cr and Mn also rise indicating a diffusion of those elements to the surface of the powder grains during the SLM process, while Ni is pushed away from the surface.

The peaks at 531.18 eV was attributed to chromium oxide [21]. The peak at 532.1 eV was attributed to manganese silicates and this signal increased considerably in the recycled powder (shift 1.8 eV from manganese oxide signal) [22]. The peak at 533.4 eV was associated to oxygen absorbed on the surface of the particles [23]. Nickel and iron core levels had similar intensity when comparing the virgin steel and recycled steel

Table 2
Relative changes of each core level area, taking the virgin steel powder as the reference.

Element	O	Si	Mn	Fe	Ni	Cr
ΔC (%)	32.9	7.3	20.5	156.1	−43.6	−8.1

powders. This suggests that the Ni and Fe oxidation states and concentrations near the powder grain surface are the same for both powders. All fits were analyzed by AAnalyzer software [24,25].

3.5. Surface roughness and topography

AFM topography images taken from the surface of both virgin and recycled particles are shown in Figs. 5 and 6. Data were taken from regions with no satellites after leveling the image for higher resolution and removing the noisy bars in the images and also after removing the areas with huge contrast. The surface roughness of the recycled powder particles shows a reduction compared to virgin powder as measured by AFM and calculated using the Gwyddion software [26]. The average surface roughness of recycled and virgin powder was 12 (±8) nm and 25 (±10) nm respectively measured from 4 µm² area on AFM topography images as indicated in the figure's insets. Almost same range of values were also reported by Heiden et al. with average roughness values of 10 nm and 23 nm for recycled and virgin powder particles, respectively [12]. They assigned this smoothening of recycled particles to the loss of dendrite exteriors, which leads to less friction between particles and enhances the flowability during spreading. Nevertheless, a higher repeated reuse of particles will probably increase the surface satellites and defect and will increase the roughness further. We also measured the average roughness on the polished surface of the powders mounted on mould. These samples were prepared for nanoindentation but worth of measuring the average roughness in order to analyze the bulk part of the particles. Average roughness of 6.85 (±2) nm and 9.12 (±2) nm were calculated for recycled and virgin powders, respectively. The impact of heat, oxygenation and recrystallization of particle structure during the AM processing might be the reason of such difference between the average roughness of the particles.

3.6. Nanoindentation: hardness

We performed numerous nanoindentation tests on a random selection of 10 particles of both virgin and recycled powders. Table 3 shows the average hardness of the powders measured under 250 µN for 5–10 s. The recycled powder is showing slightly higher hardness, which could probably be due to oxidation and porosity/cracks induced throughout
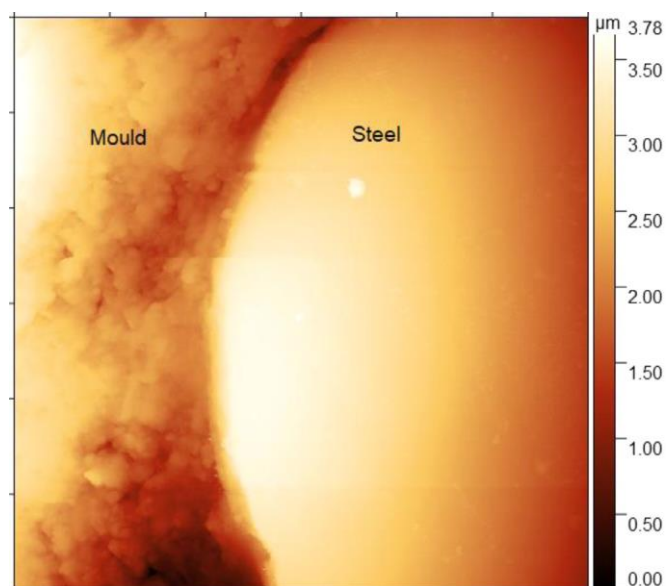

Fig. 5. the AFM topography measured from the polished surface of particles sprinkled on hard mould. The degree of roughness is notable on mould and steel surface.
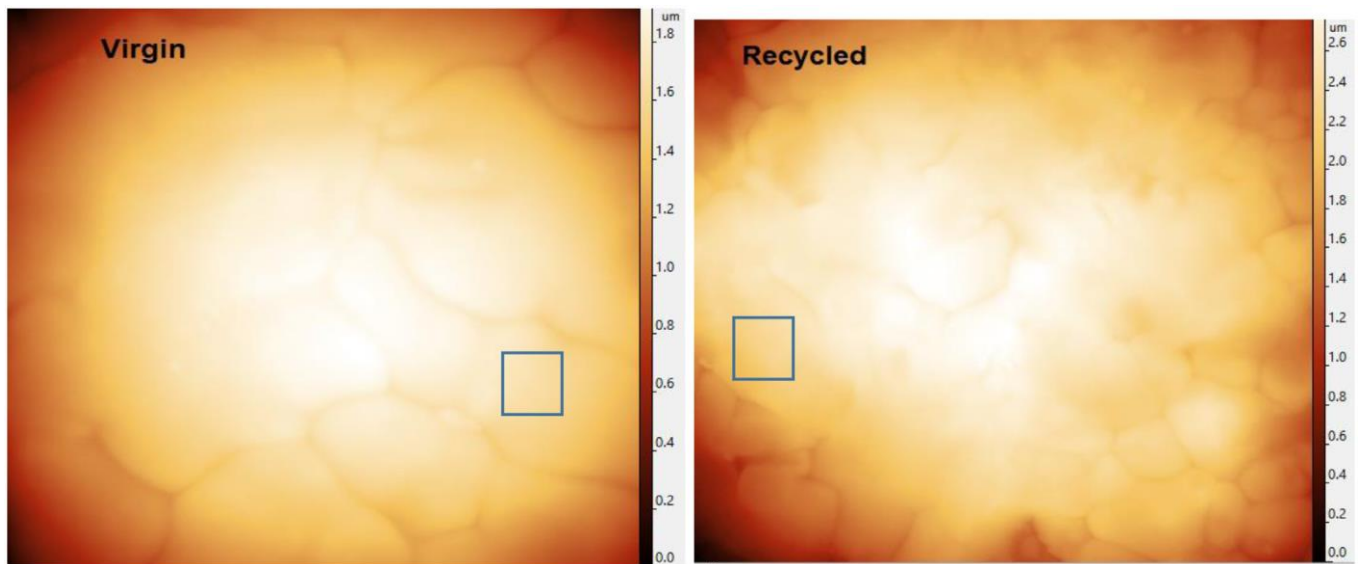
Fig. 6. Representative AFM measurement areas (4 μm^2) for a virgin and recycled particle. The roughness of the recycled powder was measured to be less than the virgin powder.

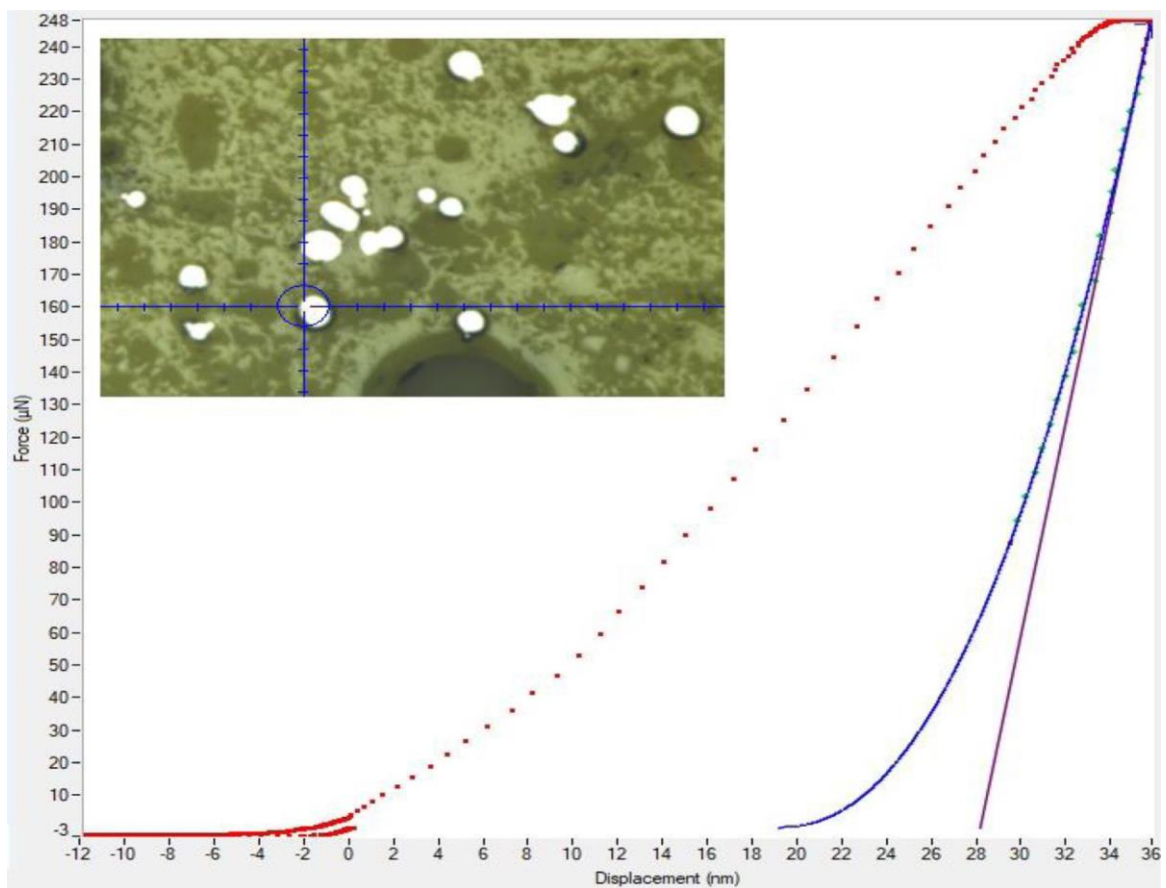**Fig. 7.** A typical plot of Force vs. Displacement from nanoindentation measurements on a recycled powder. Maximum $F = 250$ μm was applied on a randomly selected particle for 5 s. The inset shows the selected partile dispersely mounted on resin and polished as described in prevous secti on.
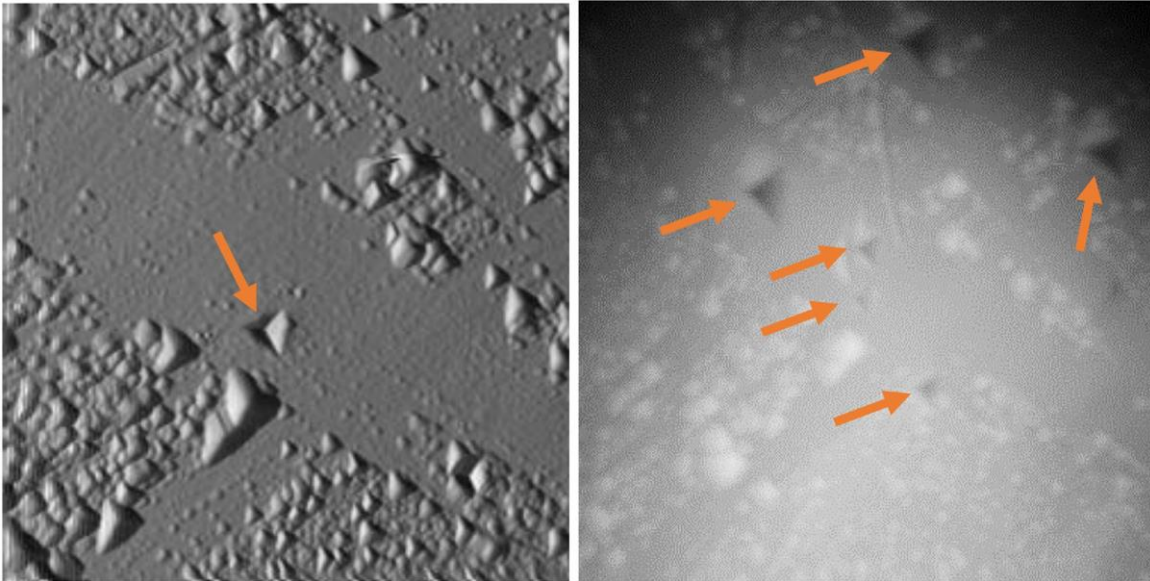
Fig. 8. Topography images of the main test indent (left) and the other indents applied on the surface of a single particle of a recycled powder. Different areas on different particles were indented and tested.

Table 3
Nanoindentation values measured from both recycled and virgin powders. Average Hardness with deviation values given in parenthesis. The values reported below our data were reported in Ref. [12].

Powder	Hardness (GPa)
Virgin	2.34 (±0.22)
Ref. [12]	2.56 (±0.21)
Recycled	3.30 (±0.36)
Ref. [12]	3.64 (±0.67)

the particle's structure during manufacturing. In fact, SEM images confirmed the presence of porosity on the surface of the powder, which could actually propagate towards the bulk of the particles. Sartin et al. reported no consistent statistical trend in microhardness but only some localized variations on the SST316L powder recycled for twelve cycles [10]. It is worth to mention that the NIST group (US) have reported almost identical hardness values for the tensile cubes made of virgin and recycled powders (11 times) [8,17]. Conversely, Heiden et al. measured slightly higher hardness on the 30 times reused powder and assigned that to higher oxidation of the recycled powder due to slightly smaller grain sizes of their recycled powder particles that introduce Hall-Petch strengthening [12]. On the other hand, higher hardness values were reported for metallic oxides [27] than its metal counterpart in the Materials Hardness Table [28]. In our XPS measurements, we detected a higher concentration of metal oxides for the recycled powder thus that could be another reason to obtain increased hardness values for the recycled powders. This either shows a good correlation of data obtained through characterization and mechanical properties measurements. A typical plot has been shown in Fig. 7 where a maximum force of 250 μN was applied on a particle selected from numerous particles mounted on the hard mould [29].

Fig. 8 shows the topography of nanoindentation applied on the surface of a single particle of recycled powders mounted on mould. Before planning a matrix of indents, we have applied different forces ranging from 100–1000 μN for 5–10 s also for different depths in order to determine if the indent point is at a reliable position. These randomly selected

powder particles were selected for their more spherecity and size under the optical imaging of the same nanoindentation machine following our previous nanoindentation measurement procedure [30]. The position of the indent was selected to be on smooth positions away from surface dendrites, pores and visible rough areas. The indent was imaged using imaging mode of the same machine. We performed indentation on different places on the particle and applied number of indents and measured the hardness values.

4. Conclusion

Recycling the metallic powder alloys from 3D printing machine for repeated use has been the discussion of additive manufacturing scientists recently. Some applications do not consider reusing the powder at all and some others try to use it for over 30 times. There is limited or no standard knowledge or protocol for such analysis yet. This is our earlier effort towards coming up with a standard method for recycling the used powder during additive manufacturing process. We have characterized virgin and recycled powders of stainless steel 316 L for microstructure, surface and bulk composition and hardness. The results show that the recycled powder has more oxidation on its surface and the higher concentration of metallic oxides. In addition, there are more surface satellites, cracks, porosity, bonded particles and clusters are observed compared to the microstructure of the virgin powder. Both powders show similar phase but slightly higher hardness has been obtained for the recycled powder. Those effects could be associate to nucleation process at the powders surface (bonds weaker with the oxygen incorporation). HAXPES results support the nanoindentation measurements by increased hardness of the recycled powder. Increased metal oxides in recycled powder was detected by XPS (both synchrotron and lab XPS) and this correlated with nanoindentation and AFM results. Our analysis opens a road towards greener, cost-effective and low waste process still with high mechanical properties for the 3D printed parts out of recycled metallic powder alloys. We will present our analysis on the manufactured parts from the fresh and recycled powder elsewhere in near future. In future investigations, we will reveal the porosity formation during the 3D printing process and the extend of porous particles in recycled powder compared to feedstock.

Declaration of Competing Interest

The authors declare that they have no known competing financial interests or personal relationships that could have appeared to influence the work reported in this paper.

Acknowledgment

References

[1] L.E. Murr, A metallographic review of 3D printing/additive manufacturing of metal and alloy products and components, Metallography, Microstructure, and Analysis 7 (2) (2018) 103–132 https://doi.org/10.1007/s13632-018-0433-6.

[2] M.L. Günther, C. Gebbe, T. Kamps, C. Seidel, G. Reinhart, Powder recycling in laser beam melting: strategies, consumption modeling and influence on resource efficiency, Production Engineering 12 (3) (2018) 377–389 https://doi.org/10.1007/s11740-018-0790-7.

[3] N.E. Gorji, R. O'Connor, D. Brabazon, XPS analysis of virgin and recycled metallic powders for 3D printing applications, ModTech International Conference - Modern Technologies in Industrial Engineering, June 2019.

[4] Pe. Nandwana, W.H. Peter, R.R. Dehoff, L.E. Lowe, M.M. Kirka, F. Medina, S.S. Babu, Recyclability study on inconel 718 and Ti-6Al-4 V Powders for use in electron beam melting, Metallurgical and Materials Transactions B 47B (1) (2016) 754–762 https://doi.org/10.1007/s11663-015-0477-9.

[5] H.P. Tang, M. Qian, N. Liu, X.Z. Zhang, G.Y. Yang, J. Wang, Effect of powder reuse times on additive manufacturing of Ti-6Al-4 V by selective electron beam melting, JOM 67 (3) (2015) 555–564 https://doi.org/10.1007/s11837-015-1300-4.

[6] M. Simonelli, C. Tuck, N.T. Aboulkhair, I. Maskery, I. Ashcroft, R.D. Wildman, R. Hague, Study on the laser spatter and the oxidation reactions during selective laser melting of 316 L Stainless steel, al-si10-mg, Metal. Mat. Transac. A 46A (2015) 3842–3852 https://doi.org/10.1007/s11661-015-2882-8.

[7] E. Jelis, M. Clemente, S. Kerwien, N.M. Ravindra, M.R. Hespos, Metallurgical and mechanical evaluation of 4340 steel produced by direct metal laser sintering, JOM 67 (3) (2015) 582–590 https://doi.org/10.1007/s11837-014-1273-8.

[8] G. Jacob, Ch. Brown, A. Donmez, S. Watson, J. Slotwinski, Effects of powder recycling on stainless steel powder and built material properties in metal powder bed fusion processes, NIST Advanced Manufacturing Series 100-6 (2016) https://doi.org/10.6028/NIST.AMS.100-6.

[9] B.A. Hann, Powder reuse and its effects on laser based powder fusion additive manufactured alloy, SAE International 9 (2) (2016) 209–2014 01 2071 http://doi:10.4271/2016-01-2071 .

[10] B. Sartin, T. Pond, B. Griffith, W. Everhart, L. Elder, E. Wenski, C. Cook, D. Wieliczka, W. King, A. Rubenchik, S. Wu, B. Brown, C. Johnson, J. Crow, 316 L Powder reuse for metal additive manufacturing, in: *Solid Freeform Fabrication, Proceed.* 28*th Ann. Int.*, 2017, pp. 351–365.

[11] K.L. Terrassa, J.C. Haley, B.E. MacDonald, J.M. Schoenung, Reuse of powder feedstock for directed energy deposition, Powder Technol 338 (2018) 819–829 https://doi.org/10.1016/j.powtec.2018.07.065.

[12] M.J. Heiden, L.A. Deibler, J.M. Rodelas, J.R. Koepke, D.J. Tung, D.J. Saiz, B.H. Jared, Evolution of 316 L stainless steel feedstock due to laser powder bed fusion process, Additive Manufacturing 25 (2019) 84–103 https://doi.org/10.1016/j.addma.2018.10.019.

[13] D. Galicki, F. List, S.S. Babu, A. Plotkowski, H.M. Meyer, R. seals, C. Hayes, Localized changes of stainless steel powder characteristics during selective laser melting additive manufacturing, Metallurgical and Materials Transactions A 50A (3) (2019) 1582–1606 https://doi.org/10.1007/s11661-018-5072-7.

[14] B.K. Barnhart, Characterization of powder and the effects of powder reuse in selective laser melting PhD thesis, Case Western Reserve University, 2017.

[15] J.P. Rueff, J.M. Ablett, D. Ceolin, D. Prieur, Th. Moreno, V. Baledent, B. Lassalle, J.E. Rault, M. Simon, A. Shukla, The galaxies beamline at soleil synchrotron: inelastic X-ray scattering and photoelectron spectroscopy in the hard X-ray range, J. Synchrotron Rad. 22 (2015) 175 https://doi.org/10.1107/S160057751402102X.

[16] P.D. Nezhadfar, A. Soltani-Tehrani, A. Sterling, N. Tsolas, N. Shamsaei, The effects of powder recycling on the mechanical properties of additively manufactured 17-4 ph stainless steel, in: *Solid Freeform Fab. Proceed.* 29*th Ann. International*, 2018, pp. 1292–1300.

[17] J.A. Slotwinski, E.J. Garboczi, P.E. Stutzman, C.F. Ferraris, S.S. Watson, M.A. Peltz, Characterization of metal powders used for additive manufacturing, J Res Natl Inst Stand Technol 119 (2014) 460–494 http://dx.doi.org/10.6028/jres.119.018.

[18] P. Mellin, R. Shvab, A. Strondl, M. Randelius, H. Brodin, E. Hryhab, L. Nyborg, COPGLOW and xps investigation of recycled metal powder for selective laser melting, Powder Metallurgy 28A (3) (2017) 1–9 http://dx.doi.org/10.1080/00325899.2017.1296607.

[19] A.J. Wagner, G.M. Wolfe, D.H. Fairbrother, Reactivity of vapor-deposited metal atoms with nitrogen-containing polymers and organic surfaces studied by in situ xps, Appl Surf Sci 219 (3–4) (2003) 317–328 https://doi:10.1016/S0169-4332(03)00705-0.

[20] J. Pfrommer, A. Azarpira, A. Steigert, K. Olech, et al., Active and stable nickel-based electrocatalysts based on the zno:ni system for water oxidation in alkaline media, ChemCatChem 9 (4) (2017) 672–676 https://doi:10.1002/cctc.201600922.

[21] W. Fredrikssona, S. Malmgrena, T. Gustafssona, K. Edström, Full depth profile of passive films on 316 L stainless steel based on high resolution haxpes in combination with arxps, Appl Surf Sci 258 (2012) 5790–5797 http://doi:10.1016/j.apsusc.2012.02.099. 15.

[22] C. Byrne, B. Brennan, A. McCoy, J. Bogan, A. Brady, G. Hughes, In situ xps chemical analysis of mnsio3 copper diffusion barrier layer formation and simultaneous fabrication of metal oxide semiconductor electrical test mos structures, ACS Appl. Mater. Interfaces 8 (4) (2016) 2470–2477 http://DOI:10.1021/acsami.5b08044.

[23] L. Tang, X. Li, R. Ji, K.S. Teng, G. Tai, J. Ye, Ch. Wei, Sh.P. Lau, Bottom-up synthesis of large-scale graphene oxide nanosheets, J. Mater. Chem. 22 (12) (2012) 5676 http://DOI:10.1039/c2jm15944a.

[24] A. Herrera-Gomez, "Simultaneous data fitting in ARXPS", Internal Report, CINVESTAV-Unidad Queretaro, http://www.qro.cinvestav.mx/~aanalyzer/SimultaneousFitting.pdf.

[25] M. Yakout, M.A. Elbestawi, S.C. Veldhuis, On the characterization of stainless steel 316 L parts produced by selective laser melting, Int. J. Adv. Manuf. Technol. 95 (5–8) (2018) 1953–1974 https://doi.org/10.1007/s00170-017-1303-0.

[26] http://gwyddion.net/download.php#stable-windows.

[27] M. Takeda, T. Onishi, Sh. Nakakubo, Sh. Fujimoto, Physical properties of iron-oxide scales on si-containing steels at high temperature, Mater. Trans. 50 (9) (2009) 2242–2246 https://doi.org/10.2320/matertrans.M2009097.

[28] https://www.tedpella.com/company_html/hardness.htm.

[29] A.C.F. Crips, Nanoindentation, 3rd edition, Springer, 2002.

[30] J. Liu, J. Silveira, R. Groarke, S. Parab, H. Singh, E. McCarthy, Sh. Karazi, A. Mussatto, J. Houghtaling, I. Ul Ahad, S. Naher, D. Brabazon, Effect of powder metallurgy synthesis parameters for pure aluminium on resultant mechanical properties, International Journal of Material Forming 12 (1) (2018) 79–87 https://doi.org/10.1007/s12289-018-1408-5.